Optik 130 (2017) 123–130

Contents lists available at ScienceDirect

Optik

journal homepage: www.elsevier.de/ijleo

Original research article

Study of visibility enhancement of hazy images based on dark channel prior in polarimetric imaging

Wenfei Zhang[a,b,c], Jian Liang[a,c], Haijuan Ju[a,c], Liyong Ren[a,*], Enshi Qu[a], Zhaoxin Wu[b]

[a] Research Department of Information Photonics, Xi'an Institute of Optics and Precision Mechanics, Chinese Academy of Sciences, Xi'an 710119, China
[b] Department of Electronics Science and Technology, School of Electronic & Information Engineering, Xi'an Jiaotong University, Xi'an 710049, China
[c] University of Chinese Academy of Sciences, Beijing 100049, China

ARTICLE INFO

Article history:
Received 10 May 2016
Received in revised form 5 July 2016
Accepted 7 November 2016

Keywords:
Image enhancement
Polarimetric imaging
Scattering
Visibility and imaging

ABSTRACT

During past decades, lots of efforts on image dehazing have been made based on either computer vision or physical models. In this paper, based on the combination of the polarimetric imaging and the dark channel prior techniques, we propose a novel haze-removal method. On the one hand, the former technique ensures this method has the advantage of keeping the detailed information which might be almost vanished in hazy images; on the other hand, the latter technique provides a much easier way to precisely estimate the key parameters, such as the global atmospheric light and the degree of polarization of the airlight. Moreover, in order to realize the automatically dehazing process with our method, a dynamic bias factor is creatively introduced into the dehazing process by use of the evaluation function—Entropy, ensuring excellent dehazed image being automatically obtained while not involving any other human-computer interaction. Experimental results indicate that our dehazing method can not only enhance the visibility of the hazy images effectively, but also preserve the details considerably. In addition, it is also found that this method is useful and effective for thin, medium and dense haze conditions, and thus shows a good robustness and universality.

1. Introduction

Under hazy weather conditions, the light reflected from objects is absorbed by haze particles along the route of light, resulting in the attenuation. As for imaging, besides the signal light of interest, the camera also receives much undesired light scattered by haze particles, which is usually called the airlight [1,2]. Images taken in such conditions usually have poor visibility and low contrast, and the detailed information is always lost, as well. To enhance the quality of hazy images, lots of groups engage in exploiting new dehazing methods and algorithms.

During past decades, many kinds of methods have been developed for dehazing images. These methods can be roughly divided into two categories according to the number of images used in the dehazing process. One is based on the single image method, which can accomplish haze removal only with single image [3–5]. This kind of methods can effectively

* Correspondence to: No. 17 Xinxi Road, New Industrial Park, Xi'an Hi-Tech Industrial Development Zone, China.
E-mail address: renliy@opt.ac.cn (L. Ren).

http://dx.doi.org/10.1016/j.ijleo.2016.11.047
0030-4026/

improve the visibility and the contrast of hazy images. But sometimes some detailed information may be vanished and more computational time is cost. The other is based on the multi-image method. Among these kinds of methods, polarimetric dehazing methods are especially promising [6–12]. It is known that the degradation of the visibility of hazy images is mainly caused by the airlight mentioned above. Fortunately, the airlight is always partially polarized [13,14], and this feature can be used to estimate the radiance of it. Therefore, the quality of the image can be improved through removing the airlight radiance out. Schechner et al. [6] described the original idea of the polarimetric dehazing method in detail and adequately demonstrated that this method can effectively enhance the visibility of hazy images. Later, they focused on image visibility enhancement based on polarization and obtained very interesting results [8]. Mudge et al. [9] also involved in this field but their dehazing method is almost the same as Schechner's. Furthermore, the visibility enhancement methods based on polarization have been extended to the underwater detection [15]. So far plenty of applications demonstrate that the polarimetric dehazing methods are robust and effective for handling images with poor visibility.

In general, two key steps are involved in the polarimetric dehazing algorithms. The first step is the estimation of the global atmospheric light radiance (A_∞) which is one of the principal parameters in algorithms. The second step is the calculation of the airlight radiance (A) according to the degree of polarization (DOP) of the airlight (p_A). So the estimation of p_A is also very important. Usually, for simplicity A_∞ is estimated from the brightest patch of the hazy images, and in fact it should be the brightest pixels in the sky region. Similarly, p_A should be estimated by the pixels in the sky region. Thus the sky region should be extracted manually. It will be difficult to achieve dehazing process automatically when the images are taken randomly.

In this paper, to overcome the above drawbacks, a simple and automatic way, which is based on the dark channel prior technique, is proposed to estimate A_∞ and A. To the best of our knowledge, this is the first time to adopt the dark channel prior to estimate A in polarimetric imaging dehazing method. Furthermore, we creatively introduce a dynamic bias factor ε imposed on A_∞, which can correct the estimation inaccuracy of the transmittance of atmosphere. According to the evaluation function–Entropy, the best dehazed image can be automatically obtained while the human-computer interaction is not considered during the dehazing process.

2. Technique

2.1. Dehazing model

In general, three or four different polarization images are needed in polarimetric dehazing method. The four images scheme is utilized in our method.

In our case, four images under different angles of linear polarizer need to be captured. We fix the polarizer's angle to be 0°, 45°, 90° and 135°, and the intensities of the four images are expressed as $I(0)$, $I(45)$, $I(90)$ and $I(135)$, respectively. The Stokes matrix can be written as [16]:

$$\begin{aligned} S_0 &= I(0) + I(90) \\ S_1 &= I(0) - I(90) \\ S_2 &= I(45) - I(135) \end{aligned} \quad , \tag{1}$$

where S_0 represents the total intensity of the incident light; S_1 represents the intensity difference between the horizontal and vertical linearly polarized components; S_2 represents the intensity difference between the 45° and −45° linearly polarized components with respect to the x-axis.

The radiance received by the camera is usually expressed as $I = L{\cdot}t + A$, where $L{\cdot}t$ and A are corresponding to the direct object light radiance and the airlight radiance, respectively. L is the object light radiance in the absence of haze between the scene and the camera, which is exactly the radiance we want to obtain, and t is the transmittance of atmosphere, $t = e^{-\beta z}$. Here β is the extinction coefficient with the assumption that it is distance-invariant, and z is the distance between the scene and the camera. Meanwhile, A can be expressed as $A = A_\infty{\cdot}(1\text{-}t)$, where A_∞ is the global atmospheric light radiance. Thus, t can be given as

$$t = 1 - \frac{A}{A_\infty}. \tag{2}$$

Therefore, combining the expression of $I = L{\cdot}t + A$ and Eq. (2), L can be derived as

$$L = \frac{I - A}{1 - A/A_\infty}. \tag{3}$$

In the dehazing algorithm we have assumed that the extinction coefficient β is distance-invariant, but in fact its distance-variant property cannot be neglected. Consequently the estimated transmittance t is lower than its true value, which will lead to some unexpected brightening region in the dehazed image [7,9]. Regarding to the inaccuracy of t, a bias factor ε ($\varepsilon > 1$) is introduced to impose on A_∞. According to Eq. (2), the bias factor can increase t. Then the expression of L is modified to

$$L = \frac{I - A}{1 - A/\varepsilon A_\infty}. \tag{4}$$

Fig. 1. (a) The input haze-free image J; (b) The colour channel image of J; (c) The dark channel image of J. Here the size of $\Omega(x)$ is 13×13.

According to Eq. (4), in the whole dehazing process, we should estimate A_∞ and A efficiently and accurately. Note that the value of ε also has a significant impact on the final dehazed image quality, which will be discussed in detail in Section 3.

2.2. Key parameters estimation

The first step is to estimate A_∞. A_∞ represents the airlight radiance corresponding to an object at an infinite distance. So it should be the value of the brightest pixels in the sky region, usually for simplicity, it is estimated from the brightest patch over the whole image. However, this will lead to some mistakes when there are some extremely bright objects. So we must mark the sky region out manually. Obviously, such methods are complicated because different situations should be handled separately. Here the dark channel prior, which is verified to be effective and automatic in extracting the sky region [5], is introduced to extract the sky region in our method. The main substance is that in most of the skyless patches for haze-free images, at least one colour channel has some pixels whose intensities are very low and close to zero. As a result, the minimum intensity in such a patch is close to zero. That is to say, the dark channel image can be obtained from two minimum operators on the input image. One is the colour channel operation, which is constructed by the minimum among the values of R, G and B channel of each pixel. The other is the minimum filter operation, which is constructed from the colour channel image by selecting its minimum within a small spatial domain $\Omega(x)$ of each pixel x. Fig. 1 figuratively illustrates this phenomenon. Fig. 1(a) shows an original image J, and its corresponding colour channel and dark channel images are in Fig. 1(b) and Fig. 1(c), respectively.

In the dark channel image, the objects are obviously darker than the sky region. Due to the additional airlight, the dark channel image of hazy image is brighter than its haze-free version. So the dark channel image roughly approximates to the denseness of the haze [5]. Then the dark channel prior can be applied to detect the most haze-opaque region and extract the sky region. For avoiding the pixels located in the region with objects while the sky region is too small, the top 0.5% of the brightest pixels is picked in the dark channel image. Then the highest intensity among these pixels in the total intensity S_0 is selected as A_∞. Based on the connotation of the dark channel image, the selected pixels are mainly located in the sky region automatically. It should be pointed out that since the dark channel prior is a statistic method, it may be invalid for some particular images where some bright white objects exist and no shadow is cast on them. In our method, to avoid the influence of the noise and extremely bright white objects, we place more limitations on estimating A_∞. For the selected intensity $A_{i,j}$ at the position (i, j), the mean intensity $\bar{A}$ is obtained in the patch $\Omega(i, j)$ centered at (i, j). If each intensity $A_{m,n}$ in the patch of 13×13 around (i, j) satisfies the relationship of

$$\underset{(m,n)\in\Omega(i,j)}{|A_{m,n} - \bar{A}|} \leq \delta, \tag{5}$$

$\bar{A}$ can be selected as the real value of A_∞ in the dehazing process, i.e., $A_\infty = \bar{A}$. Otherwise the next highest intensity should be tried until the inequality (5) is satisfied.

The next step is to estimate A. The pixels selected by the dark channel prior in last step are utilized to calculate θ_A and p_A. According to the definition of the Stokes matrix and Eq. (1), the angle of polarization (θ) can be written as $\theta = \arctan(S_2/S_1)/2$. It should be noted that the calculated θ is a matrix whose size equals to that of the input image. In this matrix there are some other values which are different from θ_A. The main reason behind this point is that the object light may become partially polarized due to the scattering caused by haze particles. And the polarization orientation of the object light is inherently different from that of the airlight. For the same reason, p_A is also disturbed by the object light. Therefore, in order to eliminate the interference of the object light, we focus on the region selected by the dark channel prior and choose the mean value corresponding to such a region as the real θ_A and p_A value, i.e.,

$$\theta_A = \frac{1}{2}\left[\sum \arctan\frac{S_2(dark)}{S_1(dark)}\right]/N, \tag{6}$$

and

$$p_A = \left[\sum \frac{\sqrt{{S_1}^2(dark) + {S_2}^2(dark)}}{S_0(dark)}\right]/N, \tag{7}$$

where $S_0(\mathrm{dark})$, $S_1(dark)$ and $S_2(dark)$ represent the input S_0, S_1 and S_2 of pixels selected by the dark channel prior, respectively, and N is the number of selected pixels.

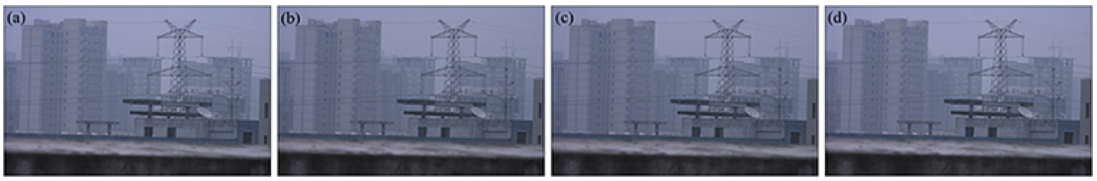

Fig. 2. Input hazy images; (a–d) are the original polarization images taken with the polarizer at the angle of 0°, 45°, 90° and 135°, respectively.

Having obtained the values of θ_A and p_A, in what follows, let us introduce the scheme for determining the value of A. For simplicity, let us define the directions of 0° and 90° as the x and y axis, respectively. Thus θ_A is the angle between the polarization orientation of the airlight and x axis. We can easily find $A_{px} = A_p \cos^2\theta_A$ and $A_{py} = A_p \sin^2\theta_A$, where A_{px} and A_{py} represent the radiance of the polarized part of the airlight in x and y direction, respectively, and A_p represents the radiance of the polarized part of the airlight. Considering the fact that A_{px} and A_{py} can be expressed as $I(0) - S_0(1-p)/2$ and $I(90) - S_0(1-p)/2$, respectively. Therefore, one can obtain the radiance of the polarized part of the airlight in θ_A direction (i.e., A_p) and there exists:

$$A_p = \frac{I(0) - S_0(1-p)/2}{\cos^2\theta_A} = \frac{I(90) - S_0(1-p)/2}{\sin^2\theta_A}, \tag{8}$$

where $p = \sqrt{{S_1}^2 + {S_2}^2}/S_0$ is the DOP of the sum radiance of the airlight and object light for each pixel over the whole images. Naturally A_p can be obtained from either $I(0)$ or $I(90)$, and then A can be easily obtained by use of $A = A_p/p_A$.

Having known all the required parameters, the object light radiance, i.e., the dehazed image can be obtained according to Eq. (4). In the whole dehazing process no additional human-computer interaction and factors on p_A and θ_A are needed.

3. Discussions of bias factor ε

In this section, we discuss the bias factor ε and introduce the evaluation function–Entropy. The experiments show that they can ensure the best dehazed image can be obtained automatically.

It should be pointed out that we have introduced a dynamic bias factor ε imposing on A_∞ in Sec. 2. And ε should be variable for different situations in which images are taken. Hence it is unreasonable to fix a certain value regardless of the specific condition. Through human-computer interaction, giving appropriate value of ε for every case, the ideal dehazing result can be obtained easily. However, this will increase the workload and computational time cost of the algorithm. To avoid the human-computer interaction step, we intend to introduce an evaluation function that can effectively represent the definition of image. There are many kinds of functions, which are usually used in the image definition assessment. According to our application and the applicability of corresponding functions, we find that the function Entropy is quite adaptive to assess the definition of dehazed images [17]. The function Entropy exhibits three perfect properties: single peak, no bias and sensitivity. All the properties of function Entropy ensure that the clearest image can be obtained. The Entropy of an image is defined as

$$Entropy = -\sum_k p_k \log_2 p_k, \tag{9}$$

where p_k is the relative frequency of gray level k. Note that the larger the Entropy value is, the clearer the image displays. Therefore, as for our method, once the largest Entropy is obtained, one can actually achieve the best dehazed image.

Now we take an example to illustrate the capacity of the evaluation function–Entropy. Four hazy images are snapped using an ordinary industrial camera with the polarizer at the angle of 0°, 45°, 90° and 135°, respectively, as shown in Fig. 2(a–d). Let us change the value of ε over the range of 1.10 to 1.60 with a step of 0.01 manually, and the dehazed images related to each ε are obtained. The Entropy is calculated for each image according to Eq. (9). Fig. 3 shows the dependence of Entropy on bias factor ε. It can be seen that the curve has only one single peak and Entropy changes significantly even for a slight change of ε of 0.01. This means Entropy is an appropriate evaluation function to estimate the dehazed images obtained by our method. The peak of Entropy is achieved when ε is 1.34. It implies that the image obtained with $\varepsilon = 1.34$ is the best one handled by our method. Meanwhile, at the top of the curve there is a wide range where the Entropies are very close. In this range the close Entropies implies that these images are almost the same, and they cannot be distinguished by human eyes, unless the difference of Entropies is large enough. In our method, we define this difference limit to be 0.3%, and those images with the Entropy difference below this limit cannot be distinguished. Note that a larger limit has ever been used in [17]. Based on our criterion of 0.3%, as shown in the inset of Fig. 3, we plot the related Entropy corresponding to ε from 1.30 to 1.41.

To compare the dehazing performance under different ε within the above criterion, in Fig. 4 we list the 12 dehazed images where ε varies from 1.30 to 1.41 with a step of 0.01. From the perspective of human, these images are all the same because their differences are beyond the resolving capability of human's eyes. Anyone of these images can be used as the dehazed

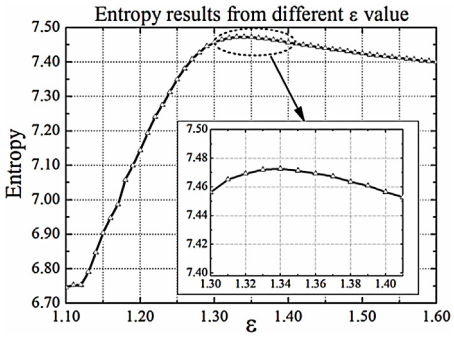

Fig. 3. Entropy versus bias factor ε for Fig. 2. The inset is the amplification of the top flat range.

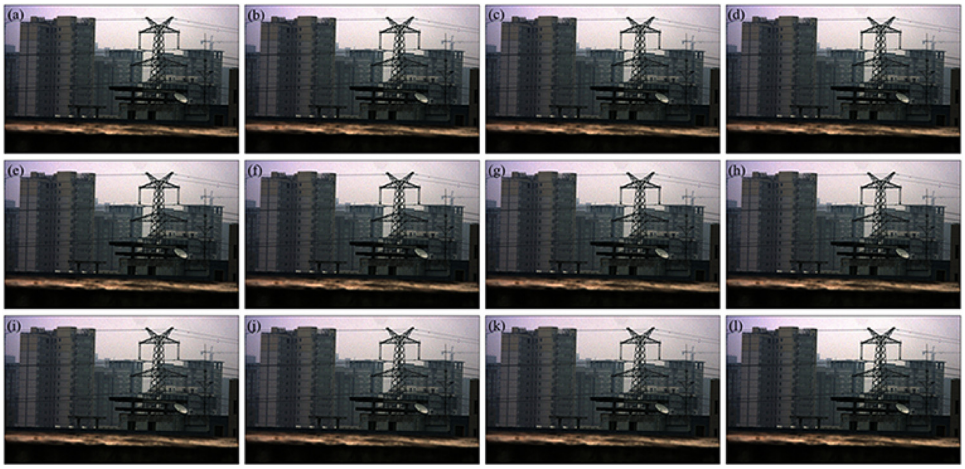

Fig. 4. (a)–(l) are the dehazed images when the bias factor ε is over the range from 1.30 to 1.41 with a step of 0.01.

Fig. 5. (a) The region marked as the red area is the pixels selected by the dark channel prior method in the dark channel image; (b) The region corresponding to that in (a) is marked as the red area in S_0 image; (c) Marked point A is the A_∞ pixels, marked point B is the brightest pixels in the whole image. (For interpretation of the references to colour in this figure legend, the reader is referred to the web version of this article.)

image result. Therefore our dehazing method has favorable tolerance, which means we can obtain a clear dehazed image easily in a wide range.

The above experiment shows that by introducing the evaluation function, the desired image can be obtained automatically through the cyclical selection of ε. After lots of experiments, we find that the best dehazed image can be obtained by our method when ε is over the range 1.10 to 1.60 for almost all the cases. Comparing to the original images Fig. 2, the visibility of the dehazed image is enhanced obviously. The contrast of Fig. 4(e) is 0.1548, and that of hazy image Fig. 2(a) is 0.1125. Here the contrast is calculated according to [18]. Meanwhile, the colour and detailed information are well preserved.

4. Results and discussion

4.1. Estimation of A_∞

In a haze-removal algorithm, no matter computer vision or polarimetric imaging, the estimation of A_∞ is a key and difficult step. We also use the images in Fig. 2 to illustrate the estimation of A_∞. The top 0.5% brightest pixels selected by the dark channel prior technique are marked as the red area in the dark channel image of Fig. 5(a). These pixels in the S_0

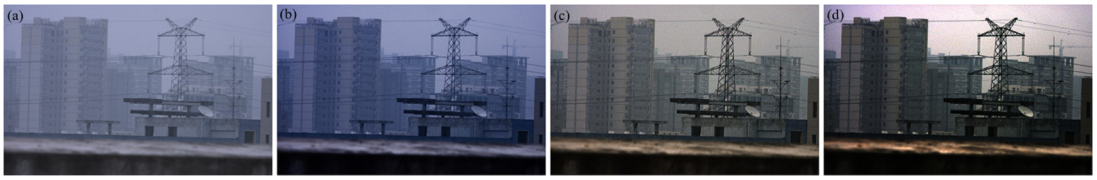

Fig. 6. Dehazing results for medium haze condition: (a) Input hazy image; (b) He's result; (c) Schechner's result; (d) Our result, here ε is 1.34.

Fig. 7. Dehazing results for thin haze condition: (a) Input hazy image; (b) He's result; (c) Schechner's result; (d) Our result, here ε is 1.21.

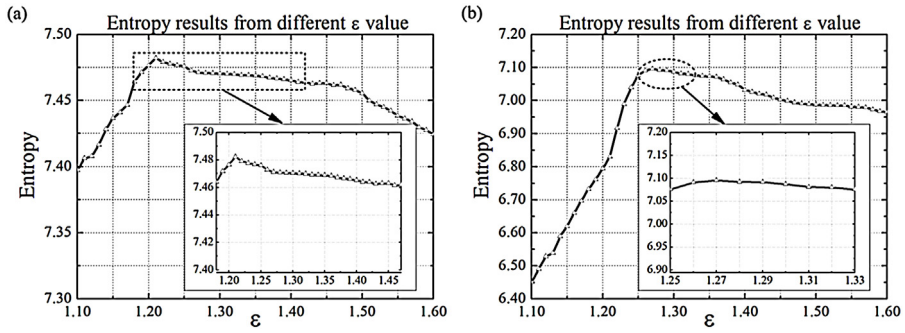

Fig. 9. (a) Entropy versus bias factor ε for Fig. 7(a). The inset is the amplification of the top flat range; (b) Entropy versus bias factor ε for Fig. 8(a). The inset is the amplification of the top flat range.

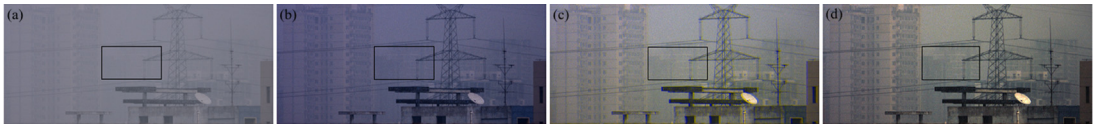

Fig. 8. Dehazing results for dense haze condition: (a) Input hazy image; (b) He's result; (c) Schechner's result; (d) Our result, here ε is 1.27.

image corresponding to Fig. 5(a) are marked as the red area in Fig. 5(b). Obviously they are all located in the sky region. According to inequality (5), A_∞ is selected and marked as point A in Fig. 5(c). It is more accurate comparing with selecting the brightest pixels in the whole image, in case some extremely bright white objects are existed in hazy image. Point B marked in Fig. 5(c) is the brightest pixels of the whole image. These pixels are not located in the sky region at all, which is obviously unreasonable. This phenomenon illustrates that the dark channel prior technique is accurate in estimating A_∞. However, it should be noted that this process is automatic and no other additional constraints are imposed on the hazy image in our method.

4.2. Experimental results

To testify the generality of our method, some experimental results handled by our method are presented. Fig. 7(a) is taken in thinner haze condition than that of Fig. 2. Fig. 7(d) shows that the dehazed image becomes perfectly distinct and nearly no haze can be found in the scene. The contrast of Fig. 7(d) is 0.3891, while in Fig. 7(a) it is only 0.1273. For the hazy image Fig. 7(a), the dependence of the curve of Entropy on ε is in Fig. 9(a). It shows that the top flat range in Fig. 9(a) is broader than that of Fig. 3. Note that this feature is consistent with the fact that haze removal in thin haze condition is much easier.

On the contray, the image in Fig. 8(a) is taken in much denser haze condition than that of Fig. 2. The dehazed image is in Fig. 8(d). Both the visibility and contrast are enhanced obviously. The buildings marked with the rectangle, which are invisible in hazy image, are even distinct. The contrast of Fig. 8(d) is 0.1363, while in Fig. 8(a) it is only 0.0808. The dependence of the curve of Entropy on ε for Fig. 8(a) is in Fig. 9(b). The top flat range is much narrower. Accordingly, only a few ε can meet the dehazing request, which means it is difficult to obtain ideal result manually. All the experimental results show that our automatic selection method is simple and effective for handing such complicate situation.

Table 1
[a]Evaluation results of dehazed images with different methods.

Scene No.	hazy image (a)	He's result (b)	Schechner's result (c)	our result (d)
Fig. 6	6.7133	7.0518	7.3091	7.4726
Fig. 7	6.5844	6.7423	7.3983	7.4822
Fig. 8	4.9142	5.9672	6.5950	7.0954

[a] Higher value represents a higher quality.

As a comparison, we implement Schechner's polarization-based method [7] and He's Dark Channel Prior [5] (Note that it is viewed as state-of-the-art single image dehazing method). The comparison results for images under different haze conditions are presented in Figs. 6–8, respectively. To objectively assess these results, the evaluation function—Entropy is employed, and the evaluation results are in Table 1. It shows that the qualities of the dehazed images are all improved to some extent by different methods. The images dehazed by the polarimetric dehazing method are better than the He's results. The reason for this may be that multiple images contain more information about the objects, as compared with the fact that the object signal might be difficult to recover from only one image once it is submerged by noise. Meanwhile, the proposed method outperforms Schechner's method.

5. Conclusions

Combining the polarimetric imaging technique and dark channel prior technique, we propose a novel method for enhancing the visibility of images taken in haze conditions. First, the sky region is extracted automatically by the dark channel prior technique, which can ensure the accuracy of A_∞ estimation. Second, the DOP and AOP of the airlight are calculated with the pixels selected by the dark channel prior technique. This can improve the estimation accuracy of the airlight radiance. These processes can be realized automatically operating on the whole hazy image. It means that we do not need to extract the sky region from the scene manually. Furthermore, the key point of our method is that a dynamic bias factor ε is introduced for correcting the deviation of the transmission t by use of the evaluation function–Entropy. It ensures that the best dehazed image can be finally obtained while not involving any other human-computer interaction during the dehazing process. Experiments indicate that our method can not only effectively enhance the image visibility but also preserve the details of image considerably for thin, medium and dense haze conditions. Especially for dense haze condition, the flexibility and automaticity of our method is more important and beneficial.

It should be noticed that we have assumed that the object light scattered by haze particles is non-polarized light. However, the object light scattered by haze particles may be partially polarized light, this leads to some restriction on enhancing the visibility further. More concentration should be focused on the object light property scattered by haze particles.

Acknowledgment

This work was supported by National Natural Science Foundation of China under grants 61505246, 61275149 and 61535015.

References

[1] C.F. Bohren, A.B. Fraser, At what altitude does the horizon cease to be visible, Am. J. Phys. 54 (1986) 222–227, http://dx.doi.org/10.1119/1.14659.
[2] R.C. Henry, S. Mahadev, S. Urquijo, D. Chitwood, Color perception through atmospheric haze, J. Opt. Soc. Am. A. 17 (2000) 831–3835, http://dx.doi.org/10.1364/JOSAA.17.000831.
[3] R. Fattal, Single image dehazing, ACM Trans. Graphics (TOG) 27 (72) (2008) 1, http://dx.doi.org/10.1145/1399504.1360671.
[4] C.O. Ancuti, C. Ancuti, P. Bekaert, Effective single image dehazing by fusion, Proc. IEEE Image Process. (2010) 3541–3544, http://dx.doi.org/10.1109/ICIP.2010.5651263.
[5] K.M. He, J. Sun, X.O. Tang, Single image haze removal using dark channel prior, IEEE Trans. Pattern Anal. Mach. Intell. 33 (2011) 2341–2353, http://dx.doi.org/10.1109/TPAMI.2010.168.
[6] Y.Y. Schechner, S.G. Narasimhan, S.K. Nayar, Instant dehazing of images using polarization, Proc. IEEE Comput. Vision Pattern Recog. (2001) 325–332, http://dx.doi.org/10.1109/CVPR.2001.990493.
[7] Y.Y. Schechner, S.G. Narasimhan, S.K. Nayar, Polarization-based vision through haze, Appl. Opt. 42 (2003) 511–525, http://dx.doi.org/10.1364/AO.42.000511.
[8] E. Namer, S. Shwartz, Y.Y. Schechner, Skyless polarimetric calibration and visibility enhancement, Opt. Express 17 (2009) 472–493, http://dx.doi.org/10.1364/OE.17.000472.
[9] J. Mudge, M. Virgen, Real time polarimetric dehazing, Appl. Opt. 52 (2013) 1932–1938, http://dx.doi.org/10.1364/AO.52.001932.
[10] J. Liang, L.Y. Ren, E.S. Qu, B.L. Hu, Y.L. Wang, Method for enhancing visibility of hazy images based on polarimetric imaging, Photon. Res. 2 (2014) 38–44, http://dx.doi.org/10.1364/PRJ.2.000038.
[11] J. Liang, L.Y. Ren, H.J. Ju, E.S. Qu, Y.L. Wang, Visibility enhancement of hazy images based on a universal polarimetric imaging method, J. Appl. Phys. 116 (2014) 173107, http://dx.doi.org/10.1063/1.4901244.
[12] S. Fang, X.S. Xia, H. Xing, C.W. Chen, Image dehazing using polarization effects of objects and airlight, Opt. Express 22 (2014) 19523–19537, http://dx.doi.org/10.1364/OE.22.019523.
[13] M.J. Raković, G.W. Kattawar, M. Mehrubeoglu, B.D. Cameron, L.V. Wang, S. Rastegar, G.L. Cote, Light backscattering polarization patterns from turbid media: theory and experiment, Appl. Opt. 38 (1999) 3399–3408, http://dx.doi.org/10.1364/AO.38.003399.
[14] D.B. Chenaultk, J.L. Pezzaniti, Polarization imaging through scattering media, Int. Symp. Optic. Sci. Technol. (2000) 124–133, http://dx.doi.org/10.1117/12.406619.

[15] Y.Y. Schechner, N. Karpel, Recovery of underwater visibility and structure by polarization analysis, IEEE J. Ocean. Eng. 30 (2005) 570–587, http://dx.doi.org/10.1109/JOE.2005.850871.
[16] D. Goldstein, Polarized Light, third ed., CRC Press, New York, 2011.
[17] R.C. Gonzalez, R.E.S.L. Woodsk Eddins, Digital Image Processing Using MATLAB, Pearson Education, 2004, 2016.
[18] R.M. Haralick, K. Shanmugam, I.H. Dinstein, Textural features for image classification, IEEE Trans. Syst. Man Cybern. 3 (1973) 610–621, http://dx.doi.org/10.1109/tsmc.1973.4309314.